Gas Permeation and Positron Annihilation Lifetime Spectroscopy of Poly(ether imides) Containing Main Chain Ethylene oxide Segments

G. C. Eastmond[1], J. Paprotny[1], R. A. Pethrick[2], and F. Santamaria-Mendia[2]

1- Department of Chemistry, Donnan Laboratory,

University of Liverpool, P.O. Box 147,

Liverpool L69 7ZD, UK,

and

2- WestCHEM, Department of Pure & Applied Chemistry,

Thomas Graham Building, University of Strathclyde,

295 Cathedral Street, G1 1XL Glasgow, UK

Abstract

This paper reports a study of four poly(ether imide)s with varying ethylene oxide [EO] segments lengths using positron annihilation lifetimes spectroscopy [PALS], wide angle X-ray diffraction and gas transport measurements. The measured properties change with the length of the EO segment. Comparison of the poly(ether imide) containing a single ether linkage with those containing one and three EO units, show progressive changes of the permeability and diffusion coefficient with void size. However when six EO units are incorporated into the polymer backbone certain of the observed trends are reversed. Incorporation of flexible EO segments in the polymer backbone allows changes the chain – chain interactions which increases the packing density and changes the void size and influences the solubility coefficients leading to variation of the gas transport characteristics. Differences in the measured solubility parameters reflect the extent to which the gases molecules are able to interact with the polymer matrix. The highest values obtained for the gas separation for carbon dioxide and nitrogen is observed when EO has a value of three. Further increasing of the length of the EO segments in the poly(ether imide) leads to a reduction the gas transport properties and hence the extent to which gas separation would be achieved.

Keywords:- positron annihilation lifetime spectroscopy, wide angel X-ray diffraction, permeability, diffusivity, solubility coefficient, poly(ether imide),

Introduction

Polyimides have been extensively investigated for use in gas permeability membranes (1-14). The problem of carbon dioxide removal from the atmosphere has highlighted two important challenges: i) achievement of good gas selectivity without sacrificing permeability and ii) maintaining the long-term gas separation performance by overcoming the problems of membrane aging and plasticization (2). Five important classes of polymer membrane materials have been identified which meet these criteria: polyimides, thermally rearranged polymers (TR's), substituted polyacetylenes, polymers with intrinsic microporosity (PIM) and polyethers (3). Changing the polymer backbone structure influences the extent to which free volume is accessible for gas transport. Varying the chemical structure and thermal treatment of the polyimides has allowed changes to be achieved in gas permeability and selectivity (1,6). Plots of gas transport parameters against the Kuhn segment size for 32 polyimides with varying chemical structures has produced curves which exhibit a maxima (4). The best transport characteristics are exhibited by polymers with Kuhn segment lengths of 60-80 angstrom, the precise value depending on the intrinsic flexibility of the back bone and the nature of the groups involved.

The poly(ether imide)s investigated in this paper, figure (1) conform to the general structure;

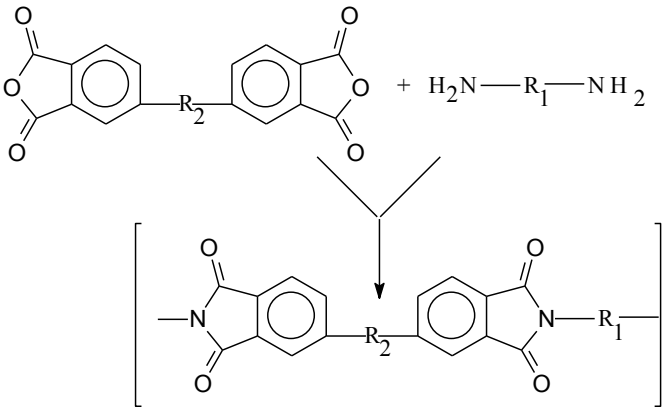

where the amine (R_1) contains an ether block with varying length:

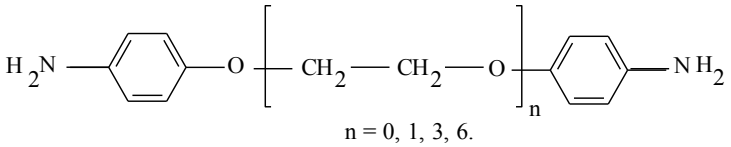

and the anhydride (R_2) has a trifluoromethyl group:

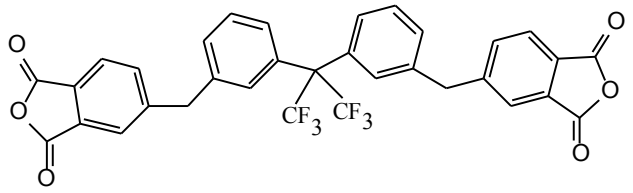

Figure (1) Schematic of poly(ether imide) synthesis and structure of the polymer studied.

The introduction of fluorine into polyimides improves solubility in organic solvents, lowers their dielectric constant and water uptake, increases their thermooxidative stability, improves their optical transparency and increases their gas permeability compared to their non-fluorinated counterparts (6,7). Polyimides containing trifluoromethyl (-CF_3) groups produced using different solvents exhibit different gas permeability's illustrating the influence of fractional free volume and segmental mobility on gas permeation in these membranes (6). Effects of thermal treatment and plasticization by the use of high-pressure CO_2 have been studied in polyimides (7). Thermal annealing causes a reduction in both the size and effective free volume leading to lower values of the permeability (8). In systems, such as hydroxyl-containing polyimides and polybenzoxazole, thermal treatment allow further reaction and chain conformational changes to occur which influences the free volume distribution as determined by positron annihilation lifetime spectroscopy – PALS (9,10). In certain polymer systems, water vapour can act as a plasticizer and influence gas diffusion by competitive sorption and void filling, reducing gas transport (11). In high barrier polymer systems, PALS indicates that the transport properties of gases can be improved by plasticization and is influenced by the free volume size distribution and the solubility of the gas (12-14). A study of 100 polyimides has shown that it is possible, in a number of cases, to correlate the permeability with the low temperature gamma relaxation and hole size as determined by PALS (13,14).

In a previous paper, we reported the glass transition -T_g and low temperature dielectric relaxation behaviour of poly(ether imide)s which contain main chain ethyleneoxide - EO segments (17). Increasing the length of the $–CH_2CH_2O-$ unit lowers the T_g and with greater than three EO units, two dielectric relaxation processes were observed; one associated with the EO unit and the other with oscillatory – librational motion of the imide segment. Whilst strong interactions between neighbouring chains give rise to high values of T_g, the EO segments will be mobile and able to influence gas transport at ambient temperatures. Chain flexibility will influence the ability for the polymer chains to pack together.

The permeation process of a gas through a polymer film is described by a solution-diffusion model [18-20]. Permeation of a gas through a polymer film occurs in three stages; firstly, sorption of the gas on to the polymer surface; secondly, diffusion of the gas through the bulk polymer; and thirdly, desorption from the opposite face of the film. Permeability, *P*, can be defined by a combination of the diffusivity, *D*, and the gas solubility, S:

$$P = D.S \qquad [1]$$

At a molecular level, it is important to understand the effect that polymer chain packing has on the free volume and its distribution, as this controls the physical, mechanical and transport properties [20]. The molecular free volume is defined as the difference between the total volume and the volume occupied by the polymer molecules. The mobility of a polymer segment and movement of a diffusing species are determined by the amount of free volume in the system. The diffusing molecule can only move from one place to another when the local free volume exceeds a critical value [18,19]. The permeability and solubility are influenced by the microstructure of the polymer. In this paper we explore the gas transport properties of carbon dioxide, oxygen, nitrogen and argon through this series of poly(ether imide)s.

Experimental

Materials.

The monomers used to synthesize the poly(ether imide)s employed in this study are identified in Table 1. The synthesis of the diamines with EO units has been described previously (21).

Table (1) Structures of the anhydride and diamines used in this paper

H_2N-R_2-NH_2	Anhydride A 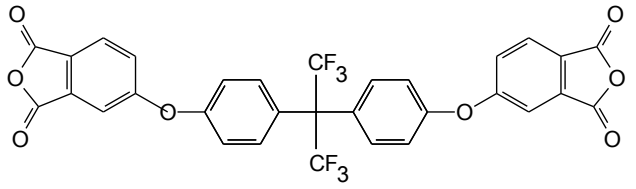
Structure	Nomenclature and code
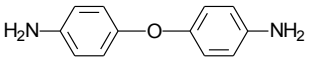	4,4'-oxydianiline – A1
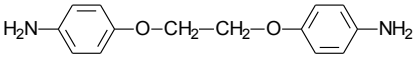	1,2-bis(4'-aminophenoxy)ethane – A2
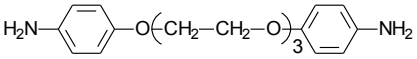	1,2-bis[2'-(4"-aminophenoxy)ethoxy]ethane – A3
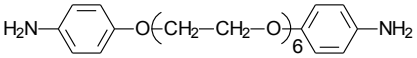	bis(2-{2'-[2"-(4"'-aminophenoxy)ethoxy]ethoxy}ethyl)ether – A4.

Bis-(4-aminophenyl)ether was obtained from Aldrich. The bis(ether anhydride),2,2-bis—[4-(2,3-dicarboxyphenoxy)phenyl]hexafluoroisopropylidine- dianhydride, were used in our previous study (22-24) Synthesis involved a nitrodisplacement reaction between 4-nitrophthalimide and 4,4'-(hexafluoroisopropylidine)diphenol (bisphenol AF) obtained from Aldrich. The resulting tetranitrile was characterized by elemental analysis and melting point. Elemental analysis: Calc. for $C_{31}H_{14}N_4O_2F_6$: C, 63.27%;H, 2.39%; N, 9.52%: Found: 63.36%; H, 2.31%; N, 9.58% Yield, 97.6%: MPt., 233-234 °C. The tetranitrile was hydrolysed to tetraacid and dehydrated to the dianhydride

which was characterized similarly. Elemental analysis: Calc. for $C_{31}H_{14}O_8F_6$: C, 59.24%;H, 2.24%: Found: C, 59.31%; H, 2.19%: Yield, 96%: MPt., 232.0-232.5 °C.

Synthesis of Polyimides. The polyimides were prepared by a conventional, two-stage solution polymerization and imidization process (22). The synthesis involved 1 mmol of diamine being dissolved in 5 cm^3 of *N*-methylpyrrolidinone (NMP) at room temperature and an exact stoichiometric equivalence of the anhydride added with stirring. After standing overnight, the mixtures formed a highly viscous solutions of poly(amic acid)s which were chemically imidized by the addition of 2 cm^3 of an equivolume mixture of acetic anhydride and pyridine at room temperature. After leaving for several hours, the resulting polyimides were isolated by precipitation into methanol. The high-molecular weight polyimides were washed with boiling precipitant to remove residual solvent. Thin films of the polymers were produced by slow solvent evaporation from polymer solutions (3 wt%) in dichloromethane in flat bottomed Petri dishes (Anumbra). The transparent, yellow films, thickness 30 – 60 μm, were annealed for 3 days at 120 °C under vacuum to remove moisture. These films were used for the gas transport, wide angel X-ray diffraction (WAXD) and PALS analysis.

Positron Annihilation Lifetime Spectroscopy [PALS].

The PALS set-up used was a state-of-the-art, fast-fast system allowing a high counting efficiency with good resolution. The scintillator used was a BaF_2 cylindrical (40 mm diameter×15 mm thick) with a Hamamatsu H2431 photo-multiplier tube (PMT's) with a borosilicate window. The front face and sides of the simulator were wrapped with PTFE tape to avoid UV reflectance and improve both time and energy resolution (25). One disadvantage of the high efficiency of BaF_2 detectors is a high probability of start-stop 'pile-up' (26) and to avoid this problem, the detectors were arranged with 90^o geometry. The scintillators were coupled to the PMT's using high viscosity (100,000 cps) silicone oil, which has a low UV absorption. The rise time of the tubes was 0.7 ns and. the configuration gave count rates of 150-300 cps and an instrument resolution of 220-240 ps FWHM for a 50 μCi source. The time to amplitude convertor used was a Canberra 2145 instrument. An epoxy encapsulated $^{22}_{11}NaCl$ source was used as the source. The source was sandwiched between layers of

the polyimide and mounted in a modified temperature controlled infrared cell. The resolution of the equipment was determined by measurement of a benzophenone single crystal and a source correction of 7.4 % @ 382 ps was used in the analysis of all PALS spectra. The lifetime components were calculated using POSITRONFIT (27,28), a least-squares analysis of the data which uses a sum of decaying exponentials to describe the lifetimes and intensity parameters. The program uses a mathematical model which expresses the polymer spectrum as a convoluted expression (symbol $*$) of the instrument resolution function and a finite number (n) of negative exponentials:

$$y(t) = R(t)^* \left(N_t \sum_{i=1}^{n} \alpha_i \lambda_i e^{-\lambda_i t} + B \right) \qquad [2]$$

where $y(t)$ is an experimental raw datum, $R(t)$ is the instrument resolution function, N_t is the normalised total count, B is the background, λ_i is the inverse of the *ith* lifetime component (τ_i), and $\alpha_i\lambda_i$ (I_i) is its intensity. An experimental spectrum $y(t)$ is fitted to equation [2] by least-squares analysis to obtain lifetimes τ_1 ($=1/\lambda_i$) and corresponding intensities $\alpha_i\lambda_i$. Experimental values of τ_1 and τ_2 were approximately 0.15 ns (*p-Ps*) and 0.41 ns (free e^+), respectively, for all samples studied and, similarly, values of I_1 and I_2 were, approximately, 19 and 65%, respectively. These values were used in the data analysis to determine values of τ_3 and I_3 *(o-Ps)* for the long-lifetime component which reflect sizes and populations of voids present. Values thus calculated for *o-Ps* lifetime and intensity were found to be virtually the same as those from a 'free' analysis.

Gas Permeability Measurements

Gas permeability was measured using a constant volume apparatus described previously (29-31). The volumes of the down and upstream stainless steel chambers were 200 cm^3. Throughout the measurement, the upstream pressure remained virtually constant and was measured using a high pressure transducer (750B MiniBaratron). The downstream pressure was monitored using a low-pressure transducer (10 Torr MKS Baratron). The polymer sample was a circular disk of 7 cm diameter. The thickness was measured on 50 points on the film using a Mitutoyo digital micrometer with a resolution of 0.1 mm. The polymer film was held between the two halves of the stainless steel cell with two flat *o*-rings providing a good seal between the membrane

and the gas cell. The sample was then de-gassed for 36 h and a leak-rate measured on the downstream side. Leak-rates of 5 mTorr per 24 hours or below were considered acceptable. A gas pressure was then introduced in the upstream side and the steady state permeation rate determined by recording the downstream transducer pressure readings. The upstream driving pressures were 4 atm. for CO_2 and N_2, 3 atm. for Ar and 2 atm. for O_2. Steady-state fluxes were obtained from pressure–time curves at times greater than three to four times the time lag, θ [29]. Calculations of pressure rise due to permeation were carried out using a Mathcad 6.0 program based on equation [3]

$$P = Jl/A\phi_p \qquad [3]$$

where, l is the membrane thickness, A is the membrane area and ϕ_p the pressure difference across the membrane. The flux, J is defined:

$$J = \left[\frac{dp}{dt}\right]\left[\frac{V}{T}\right] \qquad [4]$$

where dp/dt is the rate of change of pressure in the downstream volume, V, as a function of time and T is the temperature. Effective diffusion coefficients, D, were estimated using the film thickness, l, and the time-lag, θ , in the following relationship [29]:

$$\theta = \frac{l^2}{6D} \qquad [5]$$

The effective solubility coefficients were estimated using equation [1]. Reproducibility for identical film samples was found to be ±3–4% for the permeability coefficient, ±8–9% for the diffusion coefficient and ±10–12% for the solubility coefficient.

Density Measurements.

Densities of the cast polyimide films were determined by a flotation method at 25^0C using a saturated aqueous solution of K_2CO_3. The density of the salt solution was measured using an Anton Parr DM60 oscillating digital density meter connected to a DM601 density measuring cell. Measurements were performed in triplicate and the densiometer was thermostated at 25±0.1^{0}C. The fractional free volume was calculated using equation (6).

$$V_f = (V_T - V_0)/V_T \qquad \text{-[6]}$$

where V_T is the molar volume per repeat unit of polymer at temperature T and V_0 is the volume occupied at 0 K per mole of the repeat unit and is estimated to be 1.3 times the van der Waals volume calculated from the group contribution method of Bondi (35,36)

Wide-angle X-ray diffraction (WAXD)

Wide-angle X-ray diffraction (WAXD) measurements of the poly(ether imide)s were performed at room temperature using a Siemens D500 diffractometer which has a Cu K alpha source. Samples of polymer 9 cm square were held in an aluminium holder for analysed and were identical to those used for gas permeability measurements.

Polymer Characterization

Polymer A4 was characterized by gel permeation chromatography using DMF/LiCl(0.1 M) as eluant; other polymers were insoluble. The estimated molecular weight at the peak of the chromatogram was 66 kg mol^{-1} based on polystyrene standards, an indication of a high degree of polymerization. (32). Glass-transition temperatures (T_g's) were determined with the aid of a Perkin-Elmer DSC2 using a heating rate of 10 °C min^{-1}. T_g's quoted were obtained on the second or subsequent heating cycles and determined from the onset temperature, the apparatus uses nitrogen to heat and cool the sample. A Stanton Redcroft TG-750 thermogravimetric analyser was used to determine the onset of degradation for the poly(etherimide)s. About 0.4±0.6 mg of sample was placed in the holder and introduced into the micro-furnace. The heating rate was 108^0C min^{-1} under a flow of 10 ml min^{-1} of nitrogen. The results were plotted as weight loss versus temperature potential and the point of the initial weight loss determined.

Results and Discussion

Glass Transition Temperature and Density Data

The thermal characteristics of the polymers are summarized in table (2). The thermogravimetric analysis (TGA) showed that the polymers are stable up to temperatures over 400°C, which is significantly higher than that normally

encountered for PEO where decomposition occurs at 324-364 °C and are consistent with previous published data on poly(ether imide)s (33,34).

Table (2) Glass transition temperatures and densities for poly(ether imide)s

Polymer Code	A1	A2	A3	A4
T_g/ ^{0}C	224	194	142	92
Density /g cm^{-3}	1.402	1.405	1.389	1.371
V_f	0.163	0.153	0.148	0.142

Poly(ether imide) A1 has an ether link between the two phenyl rings of the 4,4'-oxydianiline used to create the imide rings and exhibits a T_g of 224 ^{0}C (37-39). Insertion of an –CH_2CH_2O- unit between the phenyl rings introduces an element of conformational freedom and lowers the T_g to 194 ^{o}C. Increase of the number of –CH_2CH_2O- units to three and six, further lowers the T_g to respectively 142 and 92^{0}C. The T_g of pure PEO segments are typically in the range -20^{o}C to +40^{o}C (40). In the case of these polyimides, the T_g is dictated by the strength of the polymer – polymer interactions, which in turn will influence the extent to which π-π and similar interactions are able to dictate the densification process but not necessarily the magnitude of V_f. In a previous paper (17), we showed that as the -CH_2CH_2O- content is increased there is an increase in the amplitude of the low temperature dipole relaxation associated with a limited motion of the ethyleneoxide units. This latter process is decoupled from the T_g but does allow slow stress relaxation and change in the packing density of the solid.

Wide-angle X-ray diffraction Measurements (WAXD)

The wide angle X-ray diffraction scattering spectra for the four poly(ether imide)s, figure (2), exhibit a broad diffraction peak typical of poly(imide)s. The peak in the spectra shifts with change of the length of the ether segment, table (3). The breadth of the spectra show that the poly(ether imide)s are amorphous, the maximum of the peak shifting towards higher angles as the ethylene oxide unit is extended.

Table (3). d-spacing of the poly(ether imide)s

Polyimide	d-spacing / Å	Polyimide	d-spacing / Å
A1	5.53	A2	5.43
A3	5.21	A4	4.94

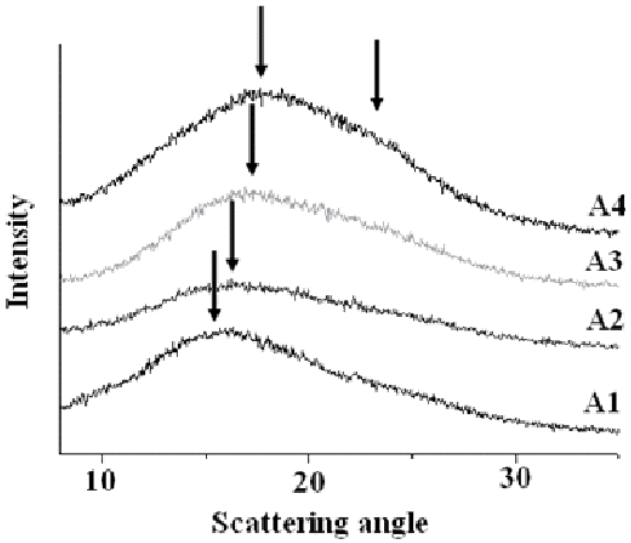

Figure (2). X-ray diffractograms of A1, A2, A3 and A4 poly(ether imide)*s*

The average interchain distance (*d*-spacing) can be used as a measure of the chain packing density and a higher value of the scattering angle corresponds to a low *d*-spacing, Table (3). The estimated distance between polymer chains is lowest for A4 and highest for A1. The *d*-spacing of A2, A3 and A4 are 1.8%, 5.7% and 10.6% respectively smaller than for A1. The shifts in the peaks are indicative of changes in the average chain separations in the polymer matrix. A tilted arrangement of aromatic units which includes the central imide group allows the terminal phenylene rings of the bis-(*N*-phenylphthalimide) units to overlap with the phthalimide groups and hence develop the charge-transfer interactions considered responsible for the strong yellow colour of many polyimides (41). The peak in A1 shifts to slightly higher angle in A2 consistent with the idea that the introduction of the ethylene oxide group is allowing closer packing of the imide groups. In A3 a shoulder is developing and clearly visible at higher angles in A4 which is consistent with the concept that a second phase is contributing to the scattering. These observations are consistent with the more detailed investigation reported previously (1) where after thermal treatment closer packing was observed.

Positron Annihilation Lifetime Spectroscopy –PALS

Numerous studies have shown the correlation between positron annihilation and gas transport **(**42-44). In poly(ether imides)s, the PALS gives rise to a long-lived component, which is a consequence of *ortho*-positronium (*o*-Ps) annihilation in amorphous regions, associated with cavities of radius 0.2–0.6 nm. (45,46). The PALS data is fitted in terms of three lifetime components: τ_1 which is attributed to *para*-positronium (*p*-Ps) annihilation; τ_2 which is associated with free positron and τ_3 which is attributed to *o*-Ps annihilation. In molecular systems, the *o*-Ps localised in a cavity annihilates through an exchange process with an electron of opposite spin associated with molecules forming the walls of the cavity and is known as the 'pick off' process. Each lifetime has a corresponding intensity (*I*) relating to the number of annihilations occurring **w**ith a particular lifetime. The long lifetime components (τ_3, I_3) therefore relate to the number and size of cavities present. The average free volume size (V_{Ps}) for a spherical cavity can be calculated (46-51):

$$V_{Ps} = \frac{4\pi R^3}{3} \qquad [8]$$

where the cavity radius, *R* is calculated from the *o*-Ps lifetime:τ_3

$$\tau_3 = \frac{1}{2}\left[1 - R(R + \Delta R) + \frac{(1)}{2\pi} sin\left(2\pi R/(R + \Delta R)\right)\right]^{-1} \qquad [9]$$

where, $\triangle R$ represents an electron layer thickness and is estimated as 0.166 nm by fitting τ_3 to known vacancy sizes of molecular crystals. Equation (7) can be used to calculate *R* from experimentally measured values of τ_3. Furthermore, the fraction of free volume, *f*, designed as the (tau x intensity product), can be found from the empirical equation:

$$f = CV_{Ps}I_3 \qquad [10]$$

where, V_{Ps} is in nm^3, I_3 in %, and *C* is an arbitrarily chosen scaling factor for a spherical cavity and depends on the chemical composition of the void walls and has typically a value of 1.5 [47]. The small changes in the chemistry of these polymers will not significantly influence the ionization potential of the polymer and hence will have only a small effect on the values measured, however the values should be considered as relative rather than absolute. The samples used for PALS, analysis

were the same membranes used for the gas permeability characterisation and density measurements. Analysis of the PALS data gave the ortho lifetimes τ_3 and intensities I_3 listed in table (4). As with the calculations of $V_{f,}$ the measured values of V_{Ps} exhibit the reverse of the trend expected in terms of the variation of T_g (48). Some variation in the values of the PALS data can be attributed to changes in the chemical structure of the void wall, however within this group of polymers these effects will not significantly influence the ionization potential of the polymer and hence should have a small effect on the values measured. However, the values reported should be considered as relative rather than absolute.

Table (4) PALS Lifetime, intensity and spherical cavity model results for the polyimides at 298 K.

Code	τ_3/ns	I_3/%	R/nm	V_{Ps}/nm^3	(τ_3^3 I_3) / (ns^3 %)
A1	1.69 $\pm$ 0.03	14.8 $\pm$ 0.3	0.255 $\pm$ 0.004	0.069 $\pm$ 0.002	71.4 $\pm$ 0.1
A2	1.41 $\pm$ 0.02	12.6 $\pm$ 0.4	0.224 $\pm$ 0.003	0.047 $\pm$ 0.01	35.3 $\pm$ 0.2
A3	1.20 $\pm$ 0.02	10.7 $\pm$ 0.2	0.197 $\pm$ 0.003	0.032 $\pm$ 0.003	18.4 $\pm$ 0.4
A4	1.25 $\pm$ 0.02	7.2 $\pm$ 0.2	0.203 $\pm$ 0.03	0.035 $\pm$ 0.003	14.0 $\pm$ 0.6

The voids detected by the PALS experiment will be influenced by the movement of the molecules which constitute the void walls (17). These librational motions are relatively small compared with the void size but could aid the diffusion of the larger gas molecules whose kinetic diameter approaches the critical value. On the time scale of the T_g processes associated with these polymers, the overall void structure may be considered to be frozen and hence V_f and V_{Ps} do not assist with the interpretation of the variation of the values of T_g which are dominated by the strength of the chain-chain interactions. The quantity (τ_3^3 I_3) is an indication of the total void content measured on a nano scale and will have a direct influence on the transport properties of gas through the membrane.

Gas Transport Measurements

The transport of gas through a membrane is influenced by a number of factors; the solubility of the gas in the membrane, hole size and the extent to which the gas can swell the matrix and influence the intrinsic local polymer dynamics. Values of the permeability and diffusion coefficients and solubility data for oxygen, carbon dioxide, nitrogen and argon in the various polymer films are listed in table (5).

Table (5) Permeability coefficients P_x, diffusion coefficients D_x and solubility coefficients S_x measured at 298K and 4 atmosphere pressure.

Polyimide code	A1	A2	A3	A4
P_{O_2}	0.9	0.32	0.17	0.21
P_{CO_2}	2.98	1.02	0.93	1.13
P_{N_2}	0.15	0.05	0.03	0.09
P_{Ar}	0.25	0.11	0.06	0.16
D_{O_2}	16.0	6.63	6.1	8.1
D_{CO_2}	4.2	2.1	2.0	4.8
D_{N_2}	4.3	1.8	1.5	4.3
D_{Ar}	4.7	2.5	1.8	5.2
S_{O_2}	5.6	4.8	2.8	2.6
S_{CO_2}	70.8	48.6	45.4	23.7
S_{N_2}	3.6	2.9	1.8	2.1
S_{Ar}	5.3	4.3	3.5	3.0

P is 10^{-10} cm^3 (STP) $cm^{-1}s^{-1}cmHg^{-1}$. (error $\pm$ 3%), D is 10^{-9} cm^2 s^{-1} (error $\pm$ 3%), S is 10^{-3} cm^3 (STP) cm^{-3} cm Hg^{-1} (error $\pm$ 3%).

The introduction of the flexible ethylene oxide (EO) linkage into the polymer backbone allows a reduction in the gas permeation coefficients for all the gases studied. However, the reduction observed in going from A1 to A3 is reversed with A4 which exhibits a higher value of the permeability compared with A3. Changing the length of the EO segment will influence the ability of neighbouring polymer chains to

interact to produce a more densely packed microstructure as noted in table (3). The variation in the permeability coefficients are shown in figure (3).

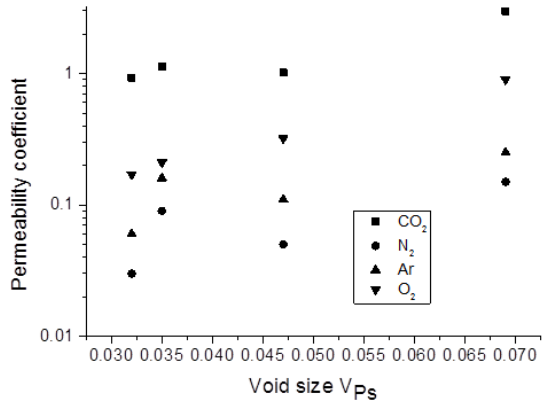

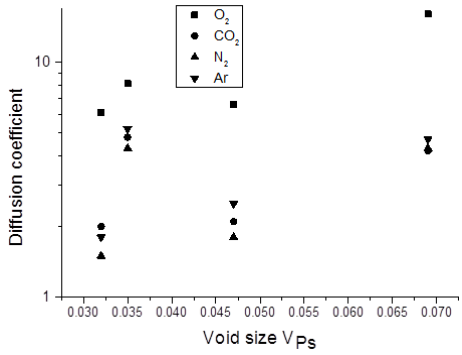

[A] [B]

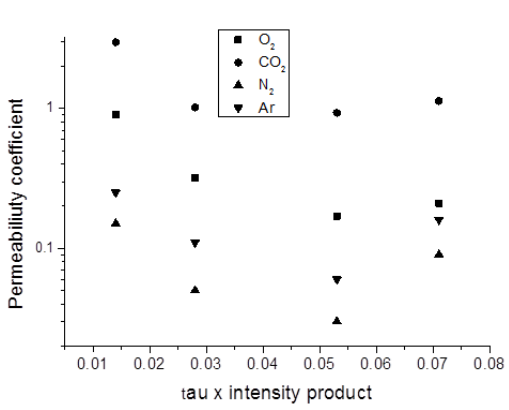

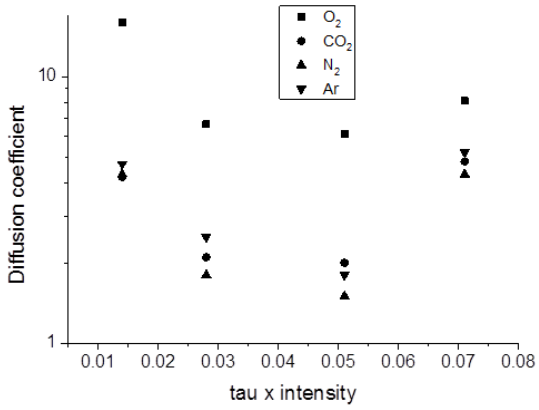

[C] [D]

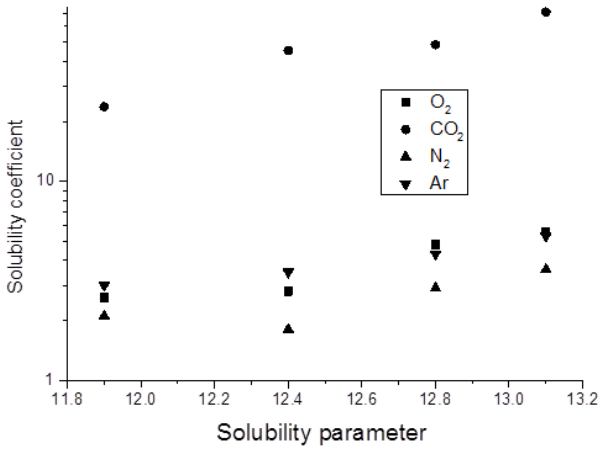

[E]

Figure (3) Permeability coefficient ($10^{-10}cm^3$(STP) $cm^{-1}s^{-1}$ cm Hg^{-1}) versus void size V_{Ps} (nm^3) [A], diffusion coefficient ($10^{-9}cm^2s^{-1}$) versus void size V_{Ps} (nm^3) [B], permeability coefficient($10^{-10}cm^3$(STP) $cm^{-1}s^{-1}$ cm Hg^{-1}) versus tau x intensity (ns^s%) [C], diffusion coefficient ($10^{-9}cm^2s^{-1}$) versus tau x intensity (ns^s%) [D], solubility coefficient (10^{-3} cm^3 (STP) $cmHg^{-1}$) versus solubility parameter ($cal^{1/2}cm^{-3/2}$) [E].

Plots of the permeability and diffusion coefficients show a progress increase with void size as determined by PALS, for carbon dioxide and oxygen. The gas permeability coefficients for A4 are higher than those for A3 reflecting the ability of the backbone chain to create both dense and more open void structures as the number of ethyleneoxide units are increased, as reflected in the X–ray data. However in the case of the diffusion coefficient, the trend appears to break down. A close examination of the data, figure (3) indicates that whilst for A1 to A3 a reduction in the diffusion coefficient with increasing EO length is observed, the values of A4 start to show a reversal. An alternative approach is to plot the permeability and diffusion coefficients against the product of the lifetime multiplied by the intensity, equation (10), which shows an initial decrease and then a finally increase. The diffusion coefficient is controlled not just by the void size but also be the number of such voids in the material. PALS measures the void size on a time scale of nano seconds and the apparent breakdown of a simple correlation may in part be attributed to the local dynamics of the matrix influencing the PALS data (50-54). For the short chains, the influence of the EO on the void size may be limited, however for EO segments containing six groups, the increased chain flexibility will allow the backbone to adopt different conformations which will influence the void size and hence the diffusion process. To fully understand the changes in the permeability one must also consider how changing the polymer structure has influenced solubility coefficient. Figure (3E) indicates the way in which the solubility coefficient S varies with the solubility parameter - δ, calculated from the group contributions using the method of Fendors (55). The values increase in a regular manner across the series as the EO content increases and this progression is followed for all the gases studied. Whilst the void size and concentration have an effect on the transport properties, the solubility of the gas in the matrix is a determining quantity. The observed values of the permeability are influenced by both diffusion and solubility.

The bridging difluoromethyl substituted methylene group in the anhydride portion of the backbone will cause the neighbouring aromatic rings to be twisted relative to one another but held in a "V" shape. The ability for other phenyl rings to undergo π-π and similar interactions will depend on how well spatially matching is achieved between neighbouring polymer chains. The introduction of the EO elements can assists these interactions being achieved by introducing flexibility along the chain, but as the EO segment increases it is possible for the chains to form microcrystalline regions. Polyimide membranes are used as separation membranes and it is appropriate to consider how the changes in the polymer structure influence the relative ease with which gases are able to be transported through the membranes (56). Table (6) summarises the relative permeability's, diffusivities and solubility's for various pairs of gases. As the size of the EO segment increases so the selectivity increases reaching a maximum value at three units before decreasing at a value of six units.

Table (6) Ratio of permeability, diffusivity and solubility for various pairs of gases.

Polyimide	A1	A2	A3	A4
P_{CO_2}/P_{O_2}	3.3	3.2	5.5	5.3
P_{CO_2}/P_{N_2}	19.3	20.5	35.9	12.3
P_{O_2}/P_{N_2}	5.9	6.3	6.6	2.3
D_{O_2}/D_{CO_2}	3.8	3.15	3.05	1.68
D_{CO_2}/D_{N_2}	1.02	1.16	1.33	1.14
D_{O_2}/D_{N_2}	3.72	3.68	4.06	1.88
S_{CO_2}/S_{O_2}	12.64	10.12	16.21	9.11
S_{CO_2}/S_{N_2}	19.66	16.75	25.22	11.28
S_{O_2}/S_{N_2}	1.55	1.65	1.55	1.23

Interestingly, the ratio of the diffusion coefficients does not parallel the permeability, the diffusion coefficient for oxygen being higher than that for carbon dioxide reflecting the relative size of the diffusing entity relative to the void size and the solubility. However the solubility coefficients indicate that the highest value is observed when there are three units in the EO segment consistent with the

permeability data. Whilst the void size is a controlling factor for diffusion, solubility in certain cases is the dominant feature influencing the permeability. This general observation is born out with the other gas ratios and supports the general contention that the structural change in the polymer allowed by the increasing flexibility of the polymer backbone not only influences the packing but also the sites for interaction with the diffusing gas molecules.

Structure of the polyimides

The introduction of the flexible ethyleneoxide groups into the backbone will allow the imide groups to move closer together and achieve a better match. The X-ray measurements indicate that the poly(ether imide) is highly amorphous, however there is an indication of a second feature appearing which reflects the possibility of more than one type of packing being created, figure (3). Whilst such ordered regions will exist on the membranes there will also be created voids associated with curved potions of the polymer backbone creating regions through which the gas molecules will be able to diffuse.

Conclusions

The introduction of ethylene oxide segments into the poly(ether imide) backbone contain a hexafluoroisopropylidine section in the anhydride precursor has very significant effects on the gas transport properties. The properties changes are progressive for changes of EO from one to three but then are reversed for EO of six. The EO units will introduce a degree of flexibility into the polymer backbone which lowers the Tg but also allows the creation of conformations which in turn influencing chain – chain packing and gas transport properties. The WAXD results confirm the free volume estimation from group contribution and the calculated values from PALS analysis; that denser packing of the polymer chains is achieved as the length of the flexible ethylene oxide unit is extended. Apparent correlations are observed between the PALS and gas transport data, but are probably influenced by the EO chain flexibility as identified previously by dielectric measurements (17), making a simple correlation of the properties not possible over all the polymers studied. The role of solubility is influencing the permeability and will be itself a function of the micro structure exposing polar sites on the polymer chain.

Acknowledgements

The authors wish to acknowledge the support of EPSRC in the form of a studentship for FSM and a post-doctoral fellowship for JP.

References

1) Stern S.A., J. Membrane Science. (1994) **94** 1-65.

2) Xiao, Y., Low, B. T., Hosseini, S. S., Chung, T. S., Paul, D. R., Progress in Polymer Science (2009) **34** (6) 561-580.

3) Du, N., Park, H. B. Dal-Cin, M. M. Guiver, M. D., Energy & Environmental Science (2012) **5** (6) 7306-7322.

4) Ronova I. A., Khokhlov A. R., Shchukin B. V., Polymer Science Series A (2007) **49** (5) 517-531

5) Dhara M.G., Banerjee S.**,** Progress in Polymer Science, (2010) **35** (8) 1022-1077

6) Cui l., Qiu, W Paul D.R., Koros W.J., Polymer 52 (2011) 3374 – 3380

7) Recio, R, Palacio, L., Pradanos, P., Hernandez A., Lozano A. E., Marcos, A., de la Campa, J. G., de Abajo, J., J. Membrane Science (2007) **293** (1-2) 22-28.

8) Duthie, X., Kentish S., Pas, S. J., Hill, A. J., Powell, C., Nagai, K., Stevens, G., Qiao, G., J. Polymer Science Part B Polymer Physics, (2008) **46 (18)** 1879-1890

9) Park C. H., Tocci E., Lee, Y. M., Drioli, E., J. Physical Chemistry B (2012) **116** (42) 12864-12877

10) Konietzny, R., Barth C., Harms, S., Raetzke, K., Koelsch, P., Staudt, C., Polymer International (2011) **60** (12) 1670-1678.

11) Sanders D.F., Smith Z.P., Guo R., Robeson L.M., McGrath J.E., Paul D.R., Freeman B.D., Polymer 54 (2013) 4729-4761

12) Mu˜noz D.M., Maya E.M., de Abajo J., de la Campa J.G., Lozano A.E., J. Membrane Science (2008) **323** 53–59.

13) Chen, G. Q., Scholes, C. A., Doherty, C. M., Hill, A., Qiao, G. G., Kentish S. E., J. Membrane Science (2012) **409** 96-104.

14) Garcia A., Iriarte M., Uriarte C., Etxeberria A., J. Membrane Science **284** (1-2) 173-179 .

15) Eastmond G. C., Paprotny J., Pethrick R. A., Santamaria-Mendia, F., Macromolecules (2006) **39** (22) 7534-7548.

16) Bas C., Mercier R., Dauwe, C., Alberola, N. D., J. Membrane Science (2010) **349** (1-2) 25-34.

17) Eastmond G. C., Paprotny J., Pethrick R. A., Santamaria-Mendia J. Polymer Science Polymer Physics 2014 **52** 1326-13

18) Vieth WR. Diffusion in and through polymers: principles and applications, Munich: Hanser, 1990

19) Naylor T. deV. Permeation properties. In: Allen G, Bevington JC, editors. Comprehensive polymer science, vol 2. Oxford: Pergamon Press, 1989.

20) Young RJ, Lovell PA. Introduction to polymers. 2nd ed. London: Chapman and Hall, 1991.

21) Eastmond, G. C., Paprotny, J., Polymer **2002**, 43, 3455.

22) Eastmond, G. C., Paprotny, J. and Webster, I, Polymer 1993 34 2865

23) Eastmond, G. C., Page, P. C. B., Paprotny, J., Richards, R. E. and Shaunak. R., Polymer 1994 35 4215.

24) Eastmond, G. C. and Paprotny, J., Macromolecules, 1995 28 2140.

25) Chang, T., Yin, D., Cao, C., Wang, S. and Liang, J., Nuc. Inst. Meth. Phys. Res., 1987, **A256**, 398,

26) Rajainmaki, H., *Appl. Phys.*, **A42**, 205, (1987)

27) Kirkegaard, P., Eldrup, M., Morgensen, O. E. and Pedersen, N. J., Computer Physics Communications, 1981, **23**, 307.

28) MacKenzie, I. M., Experimental Methods of Annihilation Time and Energy Spectrometry, Positron Solid-State Physics, (Eds: W. Brandt and A. Dupasquier), North-Holland, Amsterdam, 1983.

29) Barrer RM. Diffusion in and through solids. Cambridge: Cambridge University Press, 1941.

30) Madorsky M. M., Straus S., J. Polym. Sci. **1959**, 36, 183.

31) Fares M. M.; Hacaloglu J.; Suzer S., Eur. Polym. J. **1994**, 30, 845

32) Costa G., Eastmond G.C., Fairclough J.P.A., Paprotny J., Ryan A.J., Stagnaro P., Macromolecules 2008, 41, 1034-1040

33) Polymer Handbook (4^{th} Edition) Edited by: Brandrup, J.; Immergut, Edmund H.; Grulke, Eric A.; Abe, Akihiro; Bloch, Daniel R. (2005) John Wiley & Sons, New York.

34) Tanaka K, Katsube M, Okamoto K, Kita H, Sueoka O, Ito Y. Bull. Chem Soc Jpn (1992) **65** 1891

35) Van Krevelan Properties of Polymers, Elsevair Amsterdam (1976) 65.

36) Bondi A., J. Phys. Chem. Van Der waals Volumes and radii (1964) **68** 441.

37) Haraya K, Hwang ST. J Membr Sci (1992) **71** 13

38) Nakanishi H, Jean YC. Macromolecules (1991) **24** 6618.

39) Deng Q, Zandiehnadem H, Jean YC. Macromolecules (1992) **25** 1090.

40) Deng Q, Jean YC. Macromolecules (1993) **26** 30.

41) Z. Wang, T. Chen, J. Xu, Macromolecules, **2001,** ***34,*** 9015-9022

42) Kobayashi Y, Haraya K, Hattori S, Sasuga T. Polymer (1994) **35** 925.

43) Jean YC, Yuan J-P, Liu J, Deng Q, Yang. J Polym Sci, Polym Phys Ed (1995) **33** 2365.

44) Hill AJ, Weinhold S, Stack GM, Tant MR. Eur Polym J (1996) **32** 843.

45) Hong X, Jean YC, Yang H, Jordan SS, Koros WJ. Macromolecules (1996) **29** 7859

46) Tao SJ. J Chem Phys (1972) **56** 5499.

47) Eldrup M, Lightbody D, Sherwood JN. Chem Phys (1981) **63** 51.

48) Nakanishi H, Wong SJ, Jean YC. In: Sharma SC, editor. Positron annihilation studies of fluids. Singapore: World Science, 1988.

49) Cohen MH, Turnbull D. J Chem Phys (1959) **31** 1164.

50) McGonigle E-A., J.J. Liggat J.J., Pethrick R.A., S.D. Jenkins S.D., Daly J.H., Hayward D., Polymer 42 (2001) 2413–2426

51) Pethrick R A., Positron Annihilation – A probe for nanoscale voids and free volume, Prog. Polym. Sci., (1997) **22**, 1

52) Pethrick R.A., Jacobsen F.M., Mogensen O.E., Eldrup M., J. Chem. Soc. Faraday Trans II (1980) **76** 225- 232

53) Pethrick R.A., Malhotra B.D. (1983) Physical Review B **28** (3) 1256-1262

54) Pethrick R.A. Malhotra B.D., J. Chem. Soc. Faraday Transactions II (1982) **78** (2) 297-306.

55) Fedors R.F., Polymer Engineering and Science (1974) 14 (2) 147-154

56) Sanders D.F., Smith Z.P., Guo R., Robeson L.M., McGrath J.E., Paul D.R., Freeman B.D., Polymer 54 (2013) 4729-4761